Zeitschrift: Helvetica Physica Acta
Band: 69 (1996)
Heft: 4

Artikel: Cosmological dark matter as seen with gravitational lensing
Autor: Schneider, Peter
DOI: https://doi.org/10.5169/seals-116957

Helv Phys Acta
Vol. 69 (1996)

0018-0238/96/040373-15$1.50+0.20/0

Cosmological Dark Matter as seen with Gravitational Lensing

By Peter Schneider

Max-Planck-Institut für Astrophysik, Postfach 1523, D-85740 Garching, Germany

Abstract The distortion of images of faint high-redshift galaxies by the tidal gravitational field of mass concentrations allows to investigate the mass distribution of individual galaxy clusters, the investigation of the statistical properties of the mass distribution in galaxy halos, and the detection of dark halos without any reference to their luminosity. In addition, the statistical properties of the image distortion field on large scales can be used to infer directly the power spectrum of cosmological density fluctuations. I will outline the basic methods of this new research field in extragalactic astrophysics, and present several recent results; in particular, a high-resolution mass map of a high-redshift cluster of galaxies is presented and compared to the light distribution.

1 Introduction

Gravitational light deflection has been one of the key tests of Einstein's Theory of General Relativity. Several authors in the 1920's have pointed out that this effect may give rise to spectacular effects, such as multiple images or ring-like images of distant sources, but no one expressed his vision so clearly as Zwicky in 1937, when he claimed that the observation of the gravitational lens effect will be 'a certainty'; he also estimated the probability of a distant source to be multiply imaged to be a few tenth of a percent, very close to modern estimates, and he predicted that the lens effect will allow the determination of the mass of distant cosmic objects and, due to the magnification effect, allow deeper looks into the universe (for an account of the history of this field and for references, see Chap. 1 of Schneider, Ehlers & Falco 1992, hereafter SEF). These predictions were eventually verified when Walsh, Carswell & Weymann (1979) discovered the first lensed QSO, where two QSO

images with redshift $z_s = 1.41$, separated by $6''$, have nearly identical spectra from radio to X-ray frequencies, with a giant elliptical galaxy at redshift $z_d = 0.36$, situated in a cluster of galaxies, between the images. Today, the number of multiply-imaged QSOs is about 15; in addition, 6 ring-shaped radio images have been found, in some cases with a (lower-redshift) galaxy at the ring center (for a recent review of the observational situation, see Refsdal & Surdej 1994, and the recent proceedings edited by Kochanek & Hewitt 1996). The discovery of giant luminous arcs in 1986 by Lynds & Petrosian (1986) and Soucail et al. (1987) has shown that clusters of galaxies can act as efficient lenses; cluster lensing today is one of the most active fields of gravitational lensing (for a recent review, see Fort & Mellier 1994). Finally, the impressive demonstration (Alcock et al. 1993, Aubourg et al. 1993, Udalski et al. 1993) of the feasibility of the suggestion by Paczyński (1986) to search for compact dark objects in the halo of our Galaxy, has led to an active and successful search of Galactic microlensing events, both towards the LMC and the Galactic bulge (for a recent review, see Paczyński 1996).

These discoveries have opened up a new road towards investigating massive structures in the universe. Since gravitational light deflection is insensitive to the nature and physical state of the deflecting mass, it is ideally suited to study dark matter in the universe. In this review, I will concentrate on the detection and measurement of dark halos of galaxy size or larger, using the techniques of weak lensing.

2 What is weak lensing?

Light rays from distant sources are deflected if they pass near an intervening matter inhomogeneity. This gravitational lens effect is responsible for the well-established lens systems like multiply-imaged QSOs, (radio) 'Einstein' rings, the giant luminous arcs in clusters of galaxies, and the flux variations of stars in the LMC and the Galactic bulge seen in the searches for compact objects in our Galaxy, as mentioned above. These types of lensing events are nowadays called 'strong lensing', to distinguish it from the effects discussed here: light bundles are not only deflected as a whole, but distorted by the tidal gravitational field of the deflector. This image distortion can be quite weak and can then not be detected in individual images. However, since we are lucky to live in a Universe where the sky is full of faint distant galaxies, this distortion effect can be discovered statistically. This immediately implies that weak lensing requires excellent and deep images so that image shapes (and sizes) can be accurately measured and the number density be as high as possible to reduce statistical uncertainties. Weak gravitational lensing can be defined as using the faint galaxy population to measure the mass and/or mass distribution of individual intervening cosmic structures, or the statistical properties of their mass distribution, or to detect them in the first place, independent of the physical state or nature of the matter, or the luminosity of these mass concentrations. In addition, weak lensing can be used to infer the redshift distribution of the faintest galaxies.

In order to describe these concepts in somewhat more detail, the basic theory of gravitational lensing should briefly be recalled. The formal description of gravitational lensing

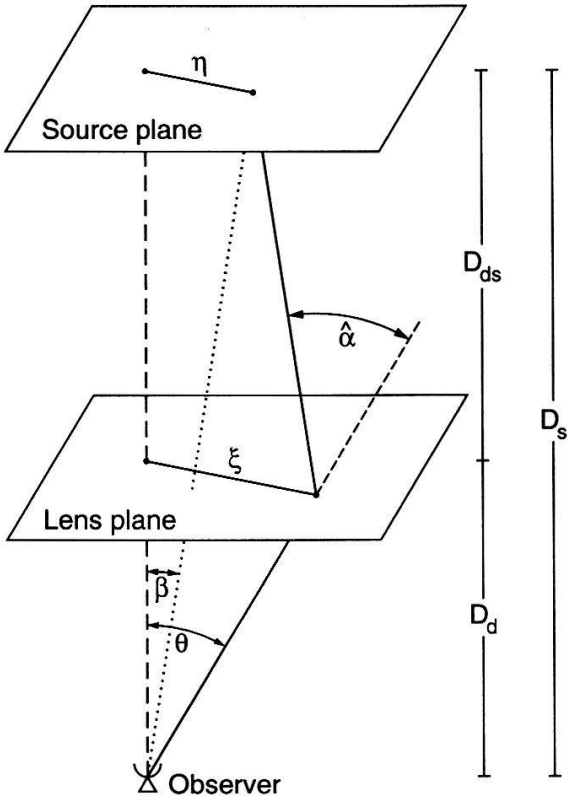

Fig. 1. The geometry of a gravitational lens

is basically simple geometry. Consider a mass distribution (the deflector) at some distance D_d from us, and some source at distance D_s (see Fig. 1). Then, draw a reference line ('optical axis') through lens and observer, define planes ('lens plane' and 'source plane') perpendicular to this optical axis through lens and source, and measure the transverse separations of a light ray in the source and lens plane by $\boldsymbol{\eta}$ and $\boldsymbol{\xi}$, respectively. Then from simple geometry, the relation between these two vectors is

$$\boldsymbol{\eta} = \frac{D_\mathrm{s}}{D_\mathrm{d}}\boldsymbol{\xi} - D_\mathrm{ds}\hat{\boldsymbol{\alpha}}(\boldsymbol{\xi}) \quad , \tag{1}$$

where $\hat{\boldsymbol{\alpha}}(\boldsymbol{\xi})$ is the *deflection angle.* Since all deflection angles one is interested in are very small (even in clusters of galaxies, the deflection angles are well below 1 arcmin), and thus the gravitational fields are weak, the *linearized field equation of General Relativity* can be employed, which implies that the deflection angle is a linear functional of the mass distribution. Since the deflection angle of a light ray passing a point mass M at separation r is $4GM/(rc^2)$, the deflection angle at position $\boldsymbol{\xi}$ caused by a mass distribution descibed by the *surface mass density* $\Sigma(\boldsymbol{\xi})$ becomes

$$\hat{\boldsymbol{\alpha}}(\boldsymbol{\xi}) = \int_{\mathbb{R}^2} \mathrm{d}^2\xi' \, \frac{4G\Sigma(\boldsymbol{\xi}')}{c^2} \, \frac{\boldsymbol{\xi} - \boldsymbol{\xi}'}{\left|\boldsymbol{\xi} - \boldsymbol{\xi}'\right|^2} \quad , \tag{2}$$

where the integral extends over the lens plane.

The simple description of a gravitational lens situation can be justified much more thoroughly from Relativity; the reader is referred to SEF, Chap. 4, and Seitz, Schneider &

Ehlers (1994) for a rigorous treatment. Here it suffices to note that for all situations encountered in this review, the gravitational lens equations provide excellent approximations; in particular, the simple geometrical derivation of (1) remains valid in a Friedmann–Lemaître universe if the distances are interpreted as *angular-diameter distances.*

It is convenient to replace the physical lengths in (1) by angular variables, by defining $\boldsymbol{\beta} = \boldsymbol{\eta}/D_\mathrm{s}$, $\boldsymbol{\theta} = \boldsymbol{\xi}/D_\mathrm{d}$,

$$\boldsymbol{\alpha}(\boldsymbol{\theta}) = \frac{D_\mathrm{ds}}{D_\mathrm{s}}\hat{\boldsymbol{\alpha}}(D_\mathrm{d}\boldsymbol{\theta}) = \frac{1}{\pi}\int_{\mathbb{R}^2} \mathrm{d}^2\theta'\, \kappa(\boldsymbol{\theta}')\frac{\boldsymbol{\theta}-\boldsymbol{\theta}'}{\left|\boldsymbol{\theta}-\boldsymbol{\theta}'\right|^2} \quad , \tag{3}$$

with the *dimensionless surface mass density*

$$\kappa(\boldsymbol{\theta}) = \frac{\Sigma(D_\mathrm{d}\boldsymbol{\theta})}{\Sigma_\mathrm{cr}} \quad \text{with} \quad \Sigma_\mathrm{cr} = \frac{c^2}{4\pi G}\frac{D_\mathrm{s}}{D_\mathrm{ds}D_\mathrm{d}} \quad ; \tag{4}$$

then the *lens equation* simply reads

$$\boldsymbol{\beta} = \boldsymbol{\theta} - \boldsymbol{\alpha}(\boldsymbol{\theta}) \quad . \tag{5}$$

The *critical surface mass density* Σ_cr is a characteristic value which separates strong from weak lenses; if $\kappa \ll 1$ everywhere (i.e., $\Sigma \ll \Sigma_\mathrm{cr}$), then the deflector is weak, whereas if $\kappa \sim 1$ for some $\boldsymbol{\theta}$, the lens may produce multiple images and is called strong. *Multiple images* occur if the lens equation (5) has multiple solutions $\boldsymbol{\theta}$ for the same source position $\boldsymbol{\beta}$.

Light bundles are not only deflected as a whole, but differential deflection occurs. Hence, in a first approximation, a circular light bundle aquires an elliptical cross section after passing a deflector. The differential deflection changes the solid angle subtended by a source. Since the *surface brightness* (or the specific intensity) is unchanged by light deflection – this follows from Liouville's theorem, or the fact that light deflection neither creates nor destroys photons – the change in solid angle leads to a change of observed flux from a source: the flux of an infinitesimally small source with surface brightness I and solid angle $\Delta\omega$ is $S = I\,\Delta\omega$. If $\Delta\omega_0$ is the solid angle subtended by an infinitesimally small source in the absence of a deflector, then the observed flux of an image of this source at $\boldsymbol{\theta}$ is $S = \mu(\boldsymbol{\theta})\,S_0$, where the *magnification* μ of an image of an infinitesimally small source is

$$\mu(\boldsymbol{\theta}) = \left|\det A(\boldsymbol{\theta})\right|^{-1} \quad , \quad \text{where} \quad A(\boldsymbol{\theta}) = \frac{\partial\boldsymbol{\beta}}{\partial\boldsymbol{\theta}} \tag{6}$$

is the Jacobian matrix of the lens equation; in components, $A_{ij} = \partial\beta_i/\partial\theta_j \equiv \beta_{i,j}$. The matrix A describes the *locally linearized lens mapping.* We can write the components of A as

$$A = \begin{pmatrix} 1-\kappa-\gamma_1 & -\gamma_2 \\ -\gamma_2 & 1-\kappa+\gamma_2 \end{pmatrix} = (1-\kappa)\mathcal{I} - |\gamma| \begin{pmatrix} \cos(2\varphi) & \sin(2\varphi) \\ \sin(2\varphi) & -\cos(2\varphi) \end{pmatrix} \quad , \tag{7}$$

where γ is called *shear* and describes the tidal gravitational forces ($\mathcal{I}$ is the two-dimensional identity matrix). The components of the shear can be calculated from (3) and (6); if we write them in complex notation, $\gamma = \gamma_1 + \mathrm{i}\gamma_2$, one finds

$$\gamma(\boldsymbol{\theta}) = \frac{1}{\pi}\int_{\mathbb{R}^2} \mathrm{d}^2\theta'\, \mathcal{D}(\boldsymbol{\theta}-\boldsymbol{\theta}')\,\kappa(\boldsymbol{\theta}') \quad , \tag{8a}$$

with the complex function

$$\mathcal{D}(\boldsymbol{\theta}) = \frac{\theta_2^2 - \theta_1^2 - 2\mathrm{i}\theta_1\theta_2}{|\boldsymbol{\theta}|^4} \quad . \tag{8b}$$

The eigenvalues of A are $1 - \kappa \pm |\gamma|$, where $|\gamma| = \sqrt{\gamma_1^2 + \gamma_2^2}$. The fact that the two eigenvalues of A will be different in general implies that a circular source will be imaged, to first approximation, into an ellipse, whose axis ratio is given by the ratio of these two eigenvalues, and the orientation of the major axis is described by the angle φ. We shall later discuss the image distortion for a general source.

Note that $\det A$ can vanish, which formally implies a diverging magnification. Of course, real magnifications remain finite. A real source is extended, and the magnification averaged over an extended source is always finite. Even if we had a point source, the magnification would remain finite: in this case, the geometrical optics approximation breaks down and light propagation had to be described by wave optics, yielding finite magnifications (see Chap. 7 of SEF). Astrophysically relevant situations involve sufficiently large sources for the geometrical optics approximation to be valid. The closed curves on which $\det A = 0$ are called *critical curves*; the corresponding curves in the source plane, obtained by inserting the critical points into the lens equation, are called *caustics*. An image close to a critical curve can have a large magnification; also, the number of images of a source changes by ± 2 if and only if the source position changes across a caustic. In this case, two images merge at the corresponding point of the critical curve, thereby brightening, and disappear once the source has crossed the caustic. The caustic is not necessarily a smooth curve, but it can develop *cusps*. A source close to, and inside a cusp has three bright images close to the corresponding point of the critical curve, whereas it has one bright image if situated just ouside the cusp.

3 Cluster mass reconstruction from weak lensing

The fact that the sky is densely covered by faint galaxy images allows the statistical study of distortions of light bundles from these high-redshift sources. The basic idea here is that the shape of a galaxy image is affected by the tidal gravitational field along its corresponding light bundle. This tidal field causes a circular galaxy to form an elliptical image. Since galaxies are not round intrinsically, this effect can not be detected in individual galaxy images (except when the distortion is so strong as to lead to the formation of arcs), but since the intrinsic orientation of galaxies can be assumed to be random, a coherent alignment of images can be detected from an ensemble of galaxies. In this and the next two subsections, we shall discuss several aspects of this general idea.

If one considers the line-of-sight towards a cluster of galaxies, one can assume that the main contribution to the tidal gravitational field along light bundles corresponding to galaxies behind the cluster comes from the cluster itself, unless there are other clusters near this line-of-sight. The tidal field, or the shear, is given by (8). Since the relation (8a) between shear and surface mass density is a convolution-type integral, it can be inverted,

e.g., by Fourier methods, to yield (Kaiser & Squires 1993)

$$\kappa(\boldsymbol{\theta}) = \frac{1}{\pi}\int_{\mathbb{R}^2} \mathrm{d}^2\theta'\, \mathcal{R}\mathrm{e}\left[\mathcal{D}^*(\boldsymbol{\theta}-\boldsymbol{\theta}')\,\gamma(\boldsymbol{\theta}')\right] + \kappa_0 \quad , \tag{9}$$

where the asterisk denotes complex conjugation, and $\mathcal{R}\mathrm{e}(x)$ is the real part of the complex variable x. Hence, if the tidal field γ can be measured, the surface mass density of the cluster can be obtained from (9) up to an overall constant. The reason for this constant to occur is that a homogeneous mass sheet does not cause any shear.

One can think of several methods to characterize the shape of a galaxy image. A convenient method is provided by using the matrix of second brightness moments,

$$Q_{ij} = \frac{\int \mathrm{d}^2\theta\, I(\boldsymbol{\theta})\,(\theta_i-\bar{\theta}_i)\,(\theta_j-\bar{\theta}_j)}{\int \mathrm{d}^2\theta\, I(\boldsymbol{\theta})} \quad , \tag{10}$$

where $I(\boldsymbol{\theta})$ is the surface brightness distribution, and $\bar{\boldsymbol{\theta}}$ is the center of light of the galaxy image, defined such that $\int \mathrm{d}^2\theta\, I(\boldsymbol{\theta})\,(\boldsymbol{\theta}-\bar{\boldsymbol{\theta}}) = 0$. Defining in analogy the tensor of second brightness moments $Q_{ij}^{(\mathrm{s})}$ of the intrinsic brightness distribution of the galaxies, one finds from the lens equation (5) and the conservation of surface brightness, $I(\boldsymbol{\theta}) = I^{(\mathrm{s})}(\boldsymbol{\beta}(\boldsymbol{\theta}))$ that $Q^{(\mathrm{s})} = A\,Q\,A$, where A is given by (7).

In the following, we shall for simplicity restrict our attention to non-critical clusters only, i.e., we shall assume that $\det A > 0$ everywhere. The reader is referred to Schneider & Seitz (1995) and Seitz & Schneider (1995) for the treatment of critical clusters. One then defines the complex ellipticity of an image as

$$\epsilon = \frac{Q_{11}-Q_{22}+2\mathrm{i}Q_{12}}{Q_{11}+Q_{22}+2\sqrt{Q_{11}Q_{22}-Q_{12}^2}} \quad , \tag{11}$$

and correspondingly the ellipticity $\epsilon^{(\mathrm{s})}$ of the intrinsic brightness profile of the galaxy in terms of $Q_{ij}^{(\mathrm{s})}$. For example, if an image has elliptical contours of axis ratio $r \le 1$, then $|\epsilon| = (1-r)/(1+r)$. From the relation $Q^{(\mathrm{s})} = A\,Q\,A$ one then derives the transformation between intrinsic and observed ellipticity (Schneider 1995)

$$\epsilon^{(\mathrm{s})} = \frac{\epsilon - g}{1 - g^*\epsilon} \quad , \tag{12}$$

where

$$g = \frac{\gamma}{1-\kappa} \tag{13}$$

is the (complex) *reduced shear*. Finally, averaging over a set of galaxy images, together with the assumption that the intrinsic ellipticity distribution is isotropic, so that $\langle\epsilon^{(\mathrm{s})}\rangle = 0$, one finds that

$$g = \langle\epsilon\rangle \quad . \tag{14}$$

Several comments have to made at this point:

(a) The definition (10) of the quadrupole moments cannot be applied to real images, as the integration extends to infinity. In order not to be completely dominated by noise, a weighting function has to be included in the integrals. However, with an angle-dependent weight function, the relation between Q and $Q^{(s)}$ no longer has a simple form and is only approximately given by $Q^{(s)} = A\,Q\,A$; the deviations from this law depend on the intrinsic brightness profile of the source and the weighting function. Even worse is the effect of seeing and an anisotropic point-spread-function (PSF), in particular if the latter is not known very precisely. Several methods to deal with these complications have been discussed in the literature (e.g., Bonnet & Mellier 1995; Kaiser, Squires & Broadhurst 1995). In particular, a calibration of the relation between ϵ and $\epsilon^{(s)}$ is obtained from numerical simulations and from applying these methods to degraded HST images. It is clear that HST images with their unprecedented angular resolution are best suited for this kind of work, and that ground-based images are much more difficult to analyse. Future ground-based observations will make use of the calibration that can be obtained from HST images, in particular if an HST field is centered on the ground-based image.

(b) The fact that the observable g has to be obtained from averaging over an ensemble of galaxy images implies that this method has a finite resolution. I.e., the averaging process is performed over the galaxy images within a certain smoothing length from the point of interest. Several methods of smoothing have been discussed (Kaiser & Squires 1993, Seitz & Schneider 1995); we prefer smoothing with Gaussian weights. Since the number of images over which the average is performed is finite, the relation $\langle\epsilon^{(s)}\rangle = 0$ is not strictly valid due to the finite width of the intrinsic ellipticity distribution; only the expectation value of $\epsilon^{(s)}$ vanishes. The smoothing length need not be kept constant, but can be adapted to the local 'strength of the signal'.

(c) It is clear from (14) that only the reduced shear is an observable, but not the shear itself as needed in the inversion equation (9). If the lens is weak in the sense $\kappa \ll 1$, then $g \approx \gamma$, and (9) can be applied directly. In general, one can replace γ in (9) by $(1-\kappa)g$, which then yields an integral equation for $\kappa(\boldsymbol{\theta})$. As shown in Seitz & Schneider (1995), this integral equation can be easily solved in a few iteration steps. If this nonlinear correction is taken into account, then $\kappa(\boldsymbol{\theta})$ is no longer determined up to an overall additive constant as implied by (9), but there exists a global invariance transformation (Schneider & Seitz 1995)

$$\kappa(\boldsymbol{\theta}) \rightarrow \lambda\kappa(\boldsymbol{\theta}) + (1-\lambda) \quad , \tag{15}$$

which leaves all image shapes invariant. This invariance transformation is the mass sheet degeneracy discussed in a different context by Gorenstein, Falco & Shapiro (1988). Of course, the allowed values of λ are restricted by the requirement that the resulting mass distribution is non-negative. Hence, this constraint always allows to obtain a lower limit on the mass. An alternative way to obtain a lower limit to the mass inside circular apertures has been discussed by Kaiser (1995a) – the so-called aperture densitometry – which also allows a rigorous estimate of the uncertainty of this lower limit. Also, if the data field is sufficiently large, one might expect that κ decreases to near zero at the boundary of the field, which then yields a plausible range for λ; this in fact is one of the arguments to demand wide-angle fields.

(d) The integral in (9) extends over the whole sky; on the other hand, data are given only on

a finite data field (CCD field) $\mathcal{U}$. If the field $\mathcal{U}$ is not sufficiently large, and the contributions of the integral (9) from outside the data field are neglected, the estimate of the surface mass density is no longer unbiased, but boundary artefacts occur. Kaiser (1995a) noticed that there exists a *local* relation between the gradient of κ and certain combinations of first derivatives of the shear components,

$$\nabla\kappa = \begin{pmatrix} \gamma_{1,1} + \gamma_{2,2} \\ \gamma_{2,1} - \gamma_{1,2} \end{pmatrix} \quad ;$$

performing averages over line integrations of this local relation allows the construction of unbiased finite-field inversion formulae (Schneider 1995, Bartelmann 1995, Seitz & Schneider 1996a, Squires & Kaiser 1996). In Seitz & Schneider (1996a), an inversion formula has been derived which filters out a particular noise component in the data which is readily identified as such, and a quantitative comparison with other inversion formulae has shown it to be the most accurate currently known direct inversion method (see also the lowest three panels in Fig. 6 of Squires & Kaiser 1996).

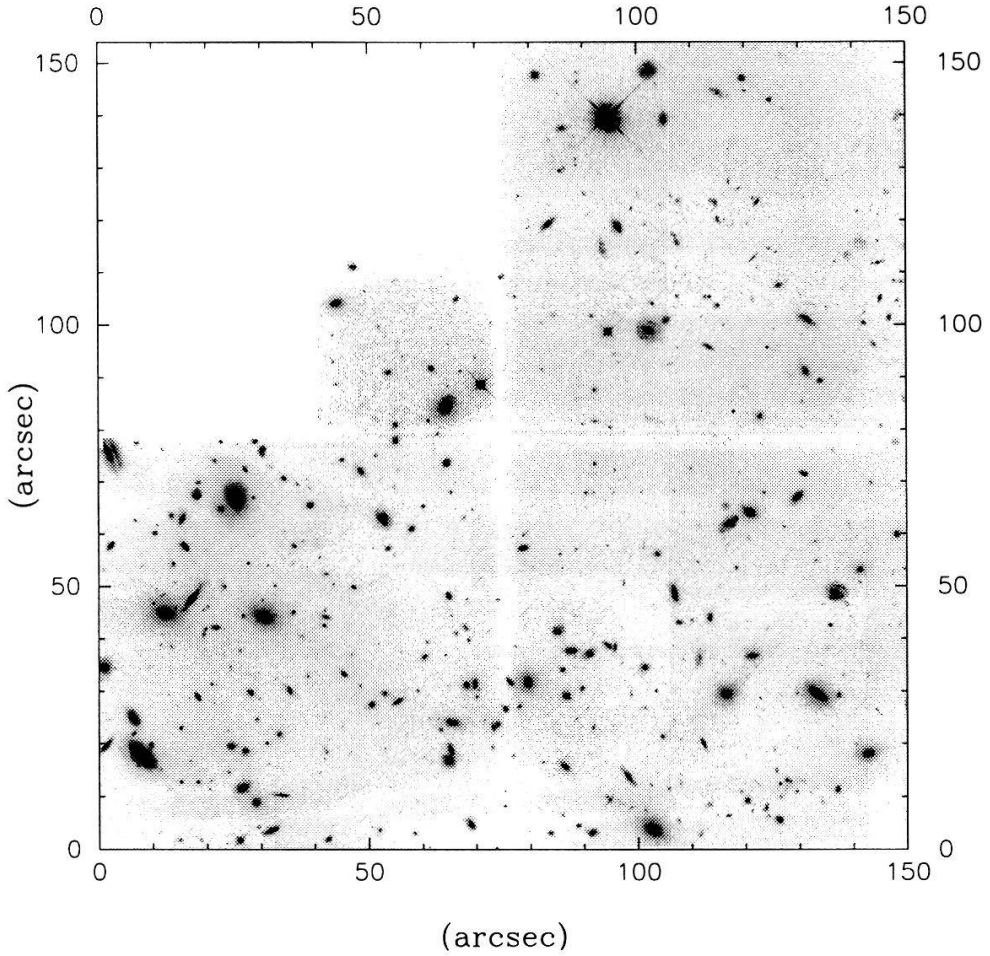

Fig. 2. The WFPC2 image of the cluster Cl0939+4713 (A851); North is at the bottom, East to the right. The coordinates are in arcseconds. The cluster center is located at about the upper left corner of the left CCD, a secondary maximum of the bright (cluster) galaxies is seen close to the interface of the two lower CCDs, and a minimum in the cluster light is at the interface between the two right CCDs. In the lensing analysis, the data from the small CCD (the Planetary Camera) were not used

(e) The transformation (15) leaves all image shapes invariant, but affects the magnification,

$\mu \to \mu/\lambda^2$. Hence, this invariance transformation can be broken if the magnification can be measured. Two possibilities have been mentioned in the literature: Broadhurst, Taylor & Peacock (1995) noticed that the magnification effect changes the local number density of galaxy images, $n(S) = n_0(S/\mu)/\mu$, where $n(S)$ are the cumulative number counts, and $n_0(S)$ are the counts in the absence of lensing. Assuming a local power law, $n_0(S) \propto S^{-\alpha}$, then $n(S)/n_0(S) = \mu^{\alpha-1}$. The blue galaxy counts have $\alpha \approx 1$, and so no magnification bias effect is observable. However, counts in the red have a flatter slope, $\alpha \approx 0.75$, and a number density decrease should be seen in regions of high magnifications. The number counts of galaxies with a red color has an even flatter slope, and the magnification effects become stronger. Indeed, this effect has been seen in the clusters A1689 (Broadhurst 1995) and Cl 0024+16 (Fort, Mellier & Dantel-Fort 1996). The magnification effect also changes the redshift distribution at fixed apparent magnitude. Bartelmann & Narayan (1995) noticed that individual galaxy images become apparently brighter, at fixed surface brightness. Assuming a sufficiently tight intrinsic magnitude - surface brightness relation, the magnification can be obtained locally. The additional information coming from the magnification effects cannot be incorporated easily in a direct inversion formula such as (9), and there are two possibilities to make use of it: one could obtain the surface mass distribution from a direct inversion, such as (9), and use the magnification information afterwards to fix the transformation parameter λ in (15). Or, one could use a reconstruction method which takes into account the *local* magnification information. One possibility for the latter is a maximum-likelihood approach (Bartelmann et al. 1996; Seitz et al. 1996, in preparation) for the reconstruction of the deflection potential ψ. For an alternative approach see Squires & Kaiser (1996).

(f) We have implicitly assumed that all sources have the same redshift, i.e., that the critical surface mass density $\Sigma_{\rm cr}$ is the same for all sources. This assumption is not too bad if the cluster is at a sufficiently low redshift, since then the ratio $D_{\rm ds}/D_{\rm s}$ can be assumed constant for faint galaxies. In general, however, the redshift distribution of galaxies has to be taken into account. In the weak lensing regime ($\kappa \ll 1$, $|\gamma| \ll 1$), only the mean value of $D_{\rm ds}/D_{\rm s}$ enters the reconstruction. The non-linear case is more complicated (Seitz & Schneider 1996b) and requires the functional form of the redshift distribution. On the other hand, this dependence may also allow to obtain constraints on the redshift distribution of the faintest galaxies. Alternatively, Bartelmann & Narayan (1995) pointed out that the expected strong dependence of surface brightness on the redshift of galaxies, together with the dependence of the lensing strength on source redshift, may allow to determine the redshift distribution of galaxies by studying the variation of lensing strength (i.e., mean ellipticity) as a function of surface brightness. Also, the comparison of lens reconstruction of clusters at different redshifts allows conclusions about the redshift distribution as a function of magnitude – see Smail, Ellis & Fitchett (1994) and in particular Luppino & Kaiser (1996) who have discovered a strong shear signal in a cluster with redshift $z = 0.83$, implying that a large fraction of the faint galaxies which show the shear effect must have a redshift well in excess of one.

The cluster construction method described above has been applied to several clusters. Fahlman et al. (1994) analyzed the shear field of the cluster MS1224 and obtained a mass-to-light ratio of $\sim 800h$, where h is the Hubble constant in units of 100 km/s/Mpc; in

particular, the mass derived is much larger than that obtained from a virial analysis. For the cluster A1689, an M/L-ratio of about $450h$ was found by two independent groups (Kaiser 1995b; Tyson & Fischer 1995). A similar value for the M/L-ratio was found for two clusters by Smail et al. (1995).

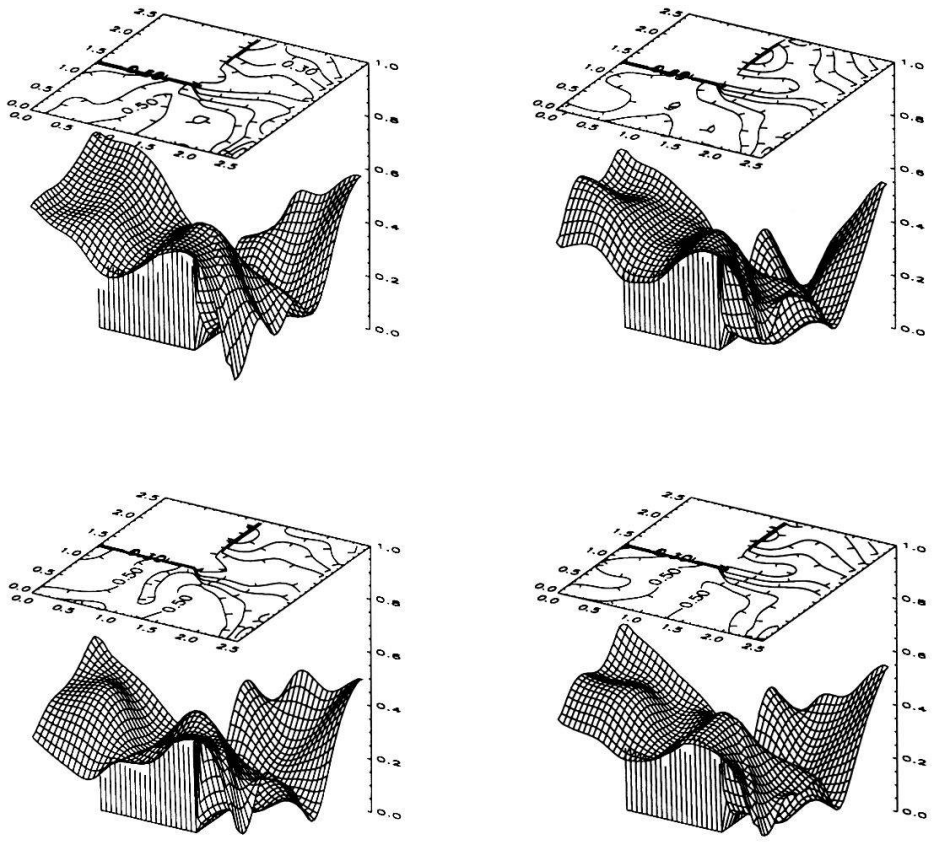

Fig. 3. The lower right panel shows the reconstructed mass distribution of A851, assuming a mean redshift of the $N = 295$ galaxies with $24 \leq R \leq 25.5$ of $\langle z \rangle = 1$. The other three panels show reconstructions obtained from the same data set via bootstrapping, i.e., selecting randomly (with replacement) $N = 295$ galaxies from the galaxy sample. The similarity of these mass distributions shows the robust features of the reconstruction, i.e., a maximum, a secondary maximum, an overall gradient, and a pronounced minimum; these features can be compared with the light distribution as shown in Fig. 2

We (Seitz et al. 1996a) have recently analyzed the 'weak' lensing effects in the cluster Cl0939+4713 (A851), using WFPC2 data (Dressler et al. 1994). Since the WFPC2 field is fairly small, we have data only in the center of the cluster, where the lensing is not weak. Also, the small field requires the use of an unbiased finite-field inversion technique, and we used the one derived in Seitz & Schneider (1996a). Fig. 2 shows the WFPC2 image of the cluster, and the reconstructed mass distribution, together with results from a bootstrapping analysis, is shown in Fig. 3. From the latter figure, one infers that the reconstruction yields basically four significant features in the mass map: a maximum close

to the position where the cluster center is predicted from optical observations, a secondary maximum roughly in the lower right CCD, an overall gradient in the lower two CCDs increasing 'to the left', and a pronounced minimum at the interface between the two right CCDs. Comparing these features with the image (Fig. 2) one sees that the maximum is clearly visible in the bright (cluster) galaxies, but also the secondary maximum and the minimum in the light distribution. In addition, the two maxima may be traced by the X-ray emission, as indicated by the ROSAT PSPC-map. Hence, in this cluster we have strong evidence of significant substructure in the mass, and that the light distribution on average follows this substructure; this has also been demonstrated quantitatively. It will be interesting to compare the mass map with a detailed HRI map which will be obtained soon (S. Schindler, private communication). The M/L-ratio of the cluster within the WFC field depends on the assumed redshift distribution of the background galaxies. Assuming that the mean redshift of galaxies with $24 \leq R \leq 25.5$ is about unity, we find that $M/L \gtrsim 200h$, a value significantly lower than for, e.g., MS1224. However, this is not too surprising, since A851 is the highest-redshift cluster in the Abell catalog which clearly biases towards high optical luminosity. In this cluster, we also have detected the magnification effect discussed above, which has allowed us to obtain not only a strict lower limit on the mass inside the data field, but also to obtain an estimate of the mass, which led to the above value for the M/L-ratio. Note, however, that this mass calibration is uncertain due to the fact that an (unknown) fraction of the faint galaxies are cluster members which renders the estimate of the magnification effect uncertain.

4 Galaxy-galaxy lensing

The shear field around clusters is sufficiently strong to measure their mass distributions – see Sect. 3. One can easily show that, assuming an isothermal mass profile, the 'detection efficiency' of a lens scales like σ^4, where σ is the velocity dispersion. This scaling then implies that individual galaxies are too weak for their presence to be detected in their shear field[1], but one should be able to detect this effect from a large ensemble of galaxies, if the signals from the individual galaxies are added statistically. The signal one would expect is a slight tangential alignment of background galaxies relative to the direction connecting this background galaxy with a near foreground galaxy.

Tyson et al. (1984) have investigated this effect using ~ 60000 galaxies; they obtained a null result. More recently, Brainerd, Blandford & Smail (1996) have analyzed a deep field; they have divided their galaxy sample into 'foreground' and 'background' galaxies, according to the optical magnitudes, and then studied the angle between the major axis of the background galaxy and the line connecting the background galaxy with the nearest foreground galaxies. The distribution of this angle shows a deficit at small angles, and an excess at large angles, indicating the expected tangential alignment. Since an accurate measurement of image ellipticities from the ground is very difficult, only galaxies brighter

[1] assuming a number density of 50 galaxies/arcmin^2, the minimum velocity dispersion for which a 3-σ detection would be possible is about 350 km/s (Miralda-Escudé 1991, Schneider & Seitz 1995).

than $r = 24$ were used; the effect disappears for fainter galaxies, which most likely shows the effect of the PSF on small images. Brainerd et al. have then simulated data, treating galaxies as truncated isothermal spheres, and distributing them in redshift, and they showed that the effect they observe is in accordance with expectations from their modelling. Recalling that this effect was detected (at a 3-σ level) with 'only' 506 'background' galaxies, it appears that one can use galaxy-galaxy lensing as a tool to investigate statistically the mass distribution in galaxies, since larger samples will become available soon (also, ground-based images with a smaller and/or more stable PSF will allow the use of fainter galaxies). Schneider & Rix (1996) have proposed a maximum likelihood method for the analysis of galaxy-galaxy lensing, which is very sensitive to the characteristic velocity dispersion of the galaxies, and which can also yield significant lower bounds on the halo size of galaxies. An application of this method to the many thousands of galaxies in the HST Medium Deep Survey will allow the determination of the characteristic velocity dispersion of galaxies to very high accuracy; in fact, Griffiths et al. (1996) have discovered a galaxy-galaxy lensing signal in the MDS. To determine the characteristic size of dark halos, one should use shallower, but wide-angle field survey which will become available soon.

5 Detection of (dark) matter concentrations

On wide-field images, one can search for (dark) mass concentrations by looking for statistically significant alignements of faint galaxy images. Let $w(x)$ be a weight function; one can then define an aperture mass

$$m(\mathbf{x}_0) := \int \mathrm{d}^2x\, \kappa(\mathbf{x})\, w\left(|\mathbf{x}-\mathbf{x}_0|\right) = \int \mathrm{d}^2x\, \kappa(\mathbf{x}+\mathbf{x}_0)\, w\left(|\mathbf{x}|\right) \quad , \tag{16}$$

which is the integral of κ in a circular aperture around $\mathbf{x}_0$, weighted by the function w. One can show (Kaiser et al. 1994, Schneider 1996) that m can be expressed directly in terms of the *tangential shear* $\gamma_\mathrm{t}(\mathbf{y};\mathbf{x}_0)$ *at position* $\mathbf{y}$ *relative to the point* $\mathbf{x}_0$, $\gamma_\mathrm{t}(\mathbf{y};\mathbf{x}_0) = -\mathcal{R}\mathrm{e}\left[\gamma(\mathbf{y}+\mathbf{x}_0)\mathrm{e}^{-2\mathrm{i}\varphi}\right]$, where φ is the polar angle of $\mathbf{y}$:

$$m(\mathbf{x}_0) = \int \mathrm{d}^2y\, \gamma_\mathrm{t}(\mathbf{y};\mathbf{x}_0)\, Q(|\mathbf{y}|) \quad , \tag{17}$$

where we have defined

$$Q(x) := \frac{2}{x^2}\int_0^x \mathrm{d}x'\, x'\, w(x') - w(x) \quad , \tag{18}$$

provided $\int \mathrm{d}x\, x\, w(x) = 0$; this last condition on $w(x)$ guarantees that the additive constant in (9) does not appear in (16). In the case of weak lensing, $\kappa \ll 1$, the image ellipticity ϵ at each point is an unbiased estimate of the local shear. Hence, the integral in (17) can be transformed into a sum over image ellipticities. The advantage of this approach is that the resulting quantity $m(\mathbf{x}_0)$ has well-defined statistical properties, so that the signal-to-noise ratio can be easily calculated for any chosen weight function w. The weight

function w can be optimized for maximizing the signal-to-noise ratio for a given shape of the mass profiles expected. As has been shown in Schneider (1996), this method yields the possibility to reliably detect isothermal-like mass concentrations with velocity dispersion in excess of 600 km/s, i.e., of very weak clusters of galaxies, without any reference to their luminosity. A systematic search for such (dark) mass concentrations is feasible; one only needs wide-field images of sufficient image quality. In fact, with a quite similar approach, Fort et al. (1996) and Smail & Dickinson (1996) have detected a significant shear field around several high-redshift QSOs and radio galaxies, indicating a (dark) mass in their line-of-sight.

6 Lensing by the large-scale structure

The cosmological density fluctuations out of which the structure in the universe has formed (at least in the conventional model of gravitational instability – which has received impressive support from the detection of microwave background fluctuations by COBE) can also distort the images of high-redshift galaxies. The corresponding distortions have been calculated by Blandford et al. (1991) and Kaiser (1992, and references therein), and are expected to be small; nevertheless, depending on the cosmological model, these distortions are measureable in principle, either by averaging the ellipticity of galaxy images over large fields, or by considering the two-point correlation function of galaxy ellipticities on large scales. If such an effect can be measured, it will allow a direct measurement of the power spectrum of the density fluctuations on the appropriate scales, very much like COBE has done. What is important to note is that the power spectrum of the density fluctuations in cosmogonies is normalized either by the amplitude of fluctuations in the microwave background, or by rms variations of galaxy numbers in 'big volumes'. Both of these normalizations are such that *relative density fluctuations* $\delta\rho/\rho$ are normalized. However, the lensing effect depends of $\delta\rho$, and not on the ratio $\delta\rho/\rho$. This implies that the gravitational distortion of images of background galaxies is proportional to the mean cosmic density Ω (Villumsen 1996a).

The same data from which galaxy-galaxy lensing was detected by Brainerd et al. (1996) have been used to search for the 'cosmic shear'; keeping in mind the difficulties to measure accurate ellipticities of very faint images from the ground, it is not surprising that Mould et al. (1994) did not find a statistically significant shear signal on a field of 4.'8 radius. Using the same data, but a different method for analyzing the image ellipticities (basically, giving less weight to 'small' images, which are most contaminated by the PSF), Villumsen (1996b) obtained a shear signal with a formal 5-σ significance. Further observations are needed to confirm this result; as mentioned before, the observations are very difficult to carry out, and the expected effects are so small that even tiny systematical effects which escape detection can mimic a significant detection.

7 Conclusions

Weak gravitational lensing has been demonstrated in the last two years to be an extremely powerful tool for extragalactic astronomy and cosmology. The fact that the theoretical concepts are so simple and well understood, and its insensitivity to the state and nature of the matter probed makes it a unique probe of (dark) mass in the universe on all scales – from MACHOs to the large-scale structure itself. The progress that has been made is intimately related to developments on the observational side. Realizing that we live in an era where wide-angle field cameras, space telescopes, and 10-meter class telescopes make their first appearance, it is clear that in weak lensing we have only scratched the surface: these new instrumental possiblitites will dramatically increase the rate and quality of data, allowing surveys for dark matter concentrations. The refurbishment of the HST has enabled images of faint galaxies with unprecedented image quality and resolution. These images, together with new theoretical developments, will allow us to understand better the relation between observed image shapes and the true image shapes, before degradation with a PSF. The combination of dark matter maps from weak lensing and X-ray and dynamical studies of clusters will yield fresh insight into the structure, dynamics, and history of these systems. If the systematic effects of ground-based imaging can be understood sufficiently well, we might be able to obtain the cosmic density and the power spectrum of density fluctuations directly from lensing.

I thank the organizers of this meeting for the invitation to an exciting and pleasant conference. This work was supported by the "Sonderforschungsbereich 375-95 für Astro–Teilchenphysik" der Deutschen Forschungsgemeinschaft.

References

Alcock, C. et al. 1993, Nat 365, 621.
Aubourg, E. et al. 1993, Nat 365, 623.
Bartelmann, M. 1995a, A&A 303, 643.
Bartelmann, M. & Narayan, R. 1995, ApJ 451, 60.
Bartelmann, M., Narayan, R., Seitz, S. & Schneider, P. 1996, ApJ 464, L115.
Blandford, R.D., Saust, A.B., Brainerd, T.G. & Villumsen, J.V. 1991, MNRAS 251, 600.
Bonnet, H. & Mellier, Y. 1995, A&A 303, 331.
Brainerd, T.G., Blandford, R.D. & Smail, I. 1996, ApJ, in press.
Broadhurst, T.J. 1995, in: *Dark matter*, AIP Conf. Proc. 336, eds. S.S. Holt & C.L. Bennett (New York: AIP).
Broadhurst, T.J., Taylor, A.N. & Peacock, J.A. 1995, ApJ 438, 49.
Dressler, A., Oemler, A., Butcher, H. & Gunn, J.E. 1994, ApJ 430, 107.
Fahlman, G., Kaiser, N., Squires, G. & Woods, D. 1994, ApJ 437, 56.
Fort, B. & Mellier, Y. 1994, A&AR 5, 239.
Fort, B., Mellier, Y. & Dantel-Fort, M. 1996, A&A, submitted.
Fort, B., Mellier, Y., Dantel-Fort, M., Bonnet, H. & Kneib, J.-P. 1996, A&A, in press.
Gorenstein, M.V., Falco, E.E. & Shapiro, I.I. 1988, ApJ 327, 693.

Griffiths, R.E., Casertano, S., Im, M. & Ratnatunga, K.U. 1996, preprint.
Kaiser, N. 1992, ApJ 388, 272.
Kaiser, N. 1995a, ApJ 439, L1.
Kaiser, N. 1995b, preprint (astro-ph/9509019).
Kaiser, N. & Squires, G. 1993, ApJ 404, 441.
Kaiser, N., Squires, G. & Broadhurst, T. 1995, ApJ 449, 460.
Kaiser, N., Squires, G., Fahlman, G. & Woods, D. 1994, in: *Clusters of galaxies*, eds. F. Durret, A. Mazure & J. Tran Thanh Van, Editions Frontiers.
Kochanek, C.S. & Hewitt, J.N. 1996, Editors of: *Astrophysical applications of gravitational lensing*, IAU Symp. 173, Kluwer.
Luppino, G. & Kaiser, N. 1996, preprint.
Lynds, R. & Petrosian, V. 1986, BAAS 18, 1014.
Miralda-Escudé, J. 1991, ApJ 370, 1.
Mould, J., Blandford, R., Villumsen, J., Brainerd, T., Smail, I., Small, T. & Kells, W. 1994, MNRAS 271, 31.
Paczyński, B. 1986, ApJ 304, 1.
Paczyński, B. 1996, ARA&A (in press).
Refsdal, S. & Surdej, J. 1994, Rep. Prog. Phys. 56, 117.
Schneider, P. 1995, A&A 302, 639.
Schneider, P. 1996, MNRAS, in press.
Schneider, P., Ehlers, J. & Falco, E.E. 1992, *Gravitational lenses*, Springer: New York (SEF).
Schneider, P. & Rix, H.-W. 1996, ApJ, in press.
Schneider, P. & Seitz, C. 1995, A&A 294, 411.
Seitz, C., Kneib, J.-P., Schneider, P. & Seitz, S. 1995, A&A, in press.
Seitz, C. & Schneider, P. 1995, A&A 297, 287.
Seitz, C. & Schneider, P. 1996b, A&A, in press.
Seitz, S. & Schneider, P. 1996a, A&A 305, 383.
Seitz, S., Schneider, P. & Ehlers, J. 1994, Class. Quan. Gravity 11, 2345.
Smail, I. & Dickinson, M. 1995, ApJ 455, L99.
Smail, I., Ellis, R.S. & Fitchett, M.J. 1994, MNRAS 270, 245.
Smail, I., Ellis, R.S., Fitchett, M.J. & Edge, A.C. 1995, MNRAS 273, 277.
Soucail, G., Fort, B., Mellier, Y. & Picat, J.P. 1987, A&A 172, L14.
Squires, G. & Kaiser, N. 1996, preprint.
Tyson, J.A. & Fischer, P. 1995, ApJ 446, L55.
Tyson, J.A., Valdes, F., Jarvis, J.F. & Mills Jr., A.P. 1984, ApJ 281, L59.
Udalski, A. et al. 1993, Acta Astro. 43, 289.
Villumsen, J.V. 1996a, MNRAS, in press.
Villumsen, J.V. 1995b, MNRAS, in press.
Walsh, D., Carswell, R.F. & Weymann, R.J. 1979, Nat 279, 381.